Int J Thermophys
DOI 10.1007/s10765-015-1935-y

Large-Scale Experimental Study of a Phase Change Material: Shape Identification for the Solid–Liquid Interface

Soumaya Kadri[1] · **Belgacem Dhifaoui**[1,2] ·
Yvan Dutil[3,4] · **Sadok Ben Jabrallah**[1,5] ·
Daniel R. Rousse[4]

Received: 9 March 2015 / Accepted: 6 July 2015
© Springer Science+Business Media New York 2015

Abstract This study describes the development of an experimental setup that tracks the evolution of the melting and freezing fronts of a Phase Change Material (PCM), in this case paraffin. The results obtained enable the examination of the shape and movement of the melting front of the PCM. Two modes of heat transfer were identified during the melting process: conduction when melting began and natural convection, which becomes dominant in the remainder of the cycle. Monitoring of the melt over time shows that the melt fraction, expressed as the ratio of the molten volume and solid volume, is proportional to the difference between the imposed temperature and the melting temperature. Experimental results confirm the linearity proposed by other researchers.

✉ Belgacem Dhifaoui
dhifaouib@gmail.com

Soumaya Kadri
kadri.soumaya@yahoo.fr

Yvan Dutil
yvan.dutil@teluq.ca

Sadok Ben Jabrallah
sadok.jabrallah@fsb.rnu.tn

Daniel R. Rousse
daniel.rousse@etsmtl.ca

[1] Laboratory of Energy, Heat and mass Transfer, Campus University, 1060 Tunis, Tunisia

[2] Higher Institute of Applied Science and Technology of Mateur, Univesity of Carthage, Tunis, Tunisia

[3] UER Science et Technologie, Télé-Université, 455 rue du Parvis, Quebec, QC, Canada

[4] t3e Industrial Research Chair, Ecole de technologie superieure, Montreal, QC 1100, Canada

[5] Faculty of Sciences of Bizerte, University of Carthage, 7021 Bizerte, Tunisia

Published online: 24 July 2015

Keywords Phase change material · Experimental work · Solid–liquid interface · Melting process

List of Symbols

Variables

A	Aspect ratios ($\mathrm{A = H \cdot L^{-1}}$)
c	Specific heat at constant pressure ($\mathrm{J \cdot kg^{-1} \cdot K^{-1}}$)
h_{sl}	Latent heat of melting/solidification of PCM ($\mathrm{J \cdot kg^{-1}}$)
Fo	Fourier number ($\mathrm{Fo} = \alpha \cdot \mathrm{t} \cdot \mathrm{L}^{-2}$)
H	Height of the rectangular enclosure (m)
k	Thermal conductivity ($\mathrm{W \cdot m^{-1} \cdot K^{-1}}$)
L	Length of the rectangular enclosure (m)
Ra	Rayleigh number ($\mathrm{Ra} = \mathrm{g} \cdot \beta\, (\mathrm{T_h} - \mathrm{T_m}) \cdot \mathrm{L}^3 \cdot (\alpha \cdot \nu)^{-1}$)
Ste	Stefan number ($\mathrm{Ste} = \mathrm{C} \cdot (\mathrm{T_h} - \mathrm{T_m}) \cdot \mathrm{h_{sl}^{-1}}$)
t	Time (s)
T	Temperature (°C)
V	Volume of the PCM liquid ($\mathrm{m^3}$)
V_0	Total volume of the PCM ($\mathrm{m^3}$)
x, y	Cartesian coordinates of the enclosure (m)

Greek Symbols

α	Thermal diffusivity ($\mathrm{m^2 \cdot s^{-1}}$)
β	Thermal expansion coefficient ($\mathrm{K^{-1}}$)
ν	Kinematic viscosity ($\mathrm{m^2 \cdot s^{-1}}$)
ρ	Density ($\mathrm{kg \cdot m^{-3}}$)

Subscripts

c	Cold
h	Hot
i	Insulating material
l	Liquid
m	Melting point
s	Solid

1 Introduction

As renewable energy sources gain importance in the world, the need to develop energy storage technologies becomes critical if we are to fully integrate renewables in the global energy system. Indeed, solar and wind energies are not constant and their production does not always coincide with the demand. At the same time, a significant portion of the energy consumed in the world is used to heat or cool. Given this fact, heat storage appears as a potential solution to the integration of renewable energy sources.

The utilization of phase change materials (PCM) in a heat storage system presents the advantage of providing a high density of heat storage at almost constant temperature. This makes the PCM especially suitable for building applications and industrial processes. Numerous reviews have been published in the last few years on this topic by Sharma et al. [1], Agyenim et al. [2], Baetens et al. [3], Kenisarin [4], Cabeza et al. [5], Kuznik et al. [6], Oro et al. [7], Zhou et al. [8], Waqas and Ud Din [9], and Dutil et al. [10].

Even though they present obvious advantages, phase change materials have not yet been widely deployed. A key problem is the difficulty in creating a mathematical model of their behavior due to the inherent non-linearity caused by the phase transition where all thermophysical properties change simultaneously. This is an impediment to the design and optimization of any type of PCM reservoir. This lack of optimization leads to larger systems than would be necessary or over-estimations of performances. Both issues lead to significant economic risk and cost increase.

1.1 Drawbacks of Numerical Methods

While numerical models of this phenomenon have been formulated for numerous cases and geometries over the last few decades [10], fundamental problems still remain. Indeed, the methods developed to determine the properties of PCM are questionable, and moreover, these methods often do not account for many fundamental phenomena common to PCM (supercooling, hysteresis, etc). Nevertheless, it is almost always claimed that they fit well with previously reported results that are often themselves based upon other models [11].

As stated by Hannoun et al. [12], a fundamental distinction exists between the concepts of verification and validation. Verification is the process used to control that the model equations are solved correctly. This is achieved by testing the model on problems with known analytic solutions, performing grid independence studies, and ensuring that the convergence pattern is consistent with the order of the discretization scheme. On the other hand, validation checks the applicability of the verified discretized mathematical model to a physical situation to be described.

Hannoun et al. [12] also demonstrated that the controversy about gallium and tin melting in cavities were caused by a lack of verification, not validation. Indeed, for gallium, the difference between experimental results [13–16] provided no clue to assist in the selection of the best models. Contrary to general wisdom in science, there is little trust in experiments to validate phase change transition models. Hence, most works only make a qualitative assessment of the quality of the models, which maintains a lack of confidence [11]. Accordingly, models are mainly verified among themselves [17,18].

While experimental data present shortcomings for benchmarking [17,18], the authors in the current paper consider that models should not only be compared to other models, but also to a variety of experimental data. In this context, it was decided that a high-quality experimental study was required to be used as a validation data source or as a standard reference to validate models. Given these circumstances, it was deemed best to examine the simplest of geometries: the rectangular enclosure.

1.2 Previous Experimental Work

To the best of our knowledge, the first experiment on this specific geometry was carried out in 1970 by Szekely and Chhabra [19]. The apparatus consisted of a furnace, holding partially solidified lead heated on one face, while the opposite face was cooled by an air jet. Numerous thermocouples were used to measure the temperature distribution. This pioneering work was followed by a series of experiments (Chiesa and Guthrie [20], mercury; Marshall [21], paraffin; Hale and Viskanta [22], n-octadecane). These were themselves followed by the experiment of Carey and Gebhart [23] on the melting of a vertical ice surface. The water temperature was kept between 3.9 °C and 8.4 °C to observe the bidirectional convection in water given its maximum density at 4 °C. A series of photographs enabled the measurement of both the position of the melting and the velocity of the convective flow.

In the following years, the Viskanta team (which had the most impact with 40 % of all citations on this topic) produced two other experiments on the melting of paraffin, (Van Buren and Viskanta [24] n-heptadecane; Ho and Viskanta [25] n-octodecane). While [22,25] documented the phase change by tracking the melt front, interferometry was used to measure the temperature field by [24]. Surprisingly, this is the only reference in the literature for this technique, and there is no explanation why it has not been reused in the following experiments on paraffin.

The same team then explored the fusion and solidification processes in gallium [15]. Gallium was chosen because of its anomalous behavior, its decreased density when it is solid (like water), and because it has a fusion temperature close to the ambient temperature, which simplifies the experiment. In this case, the opaque nature of the material did not allow the direct observation of the fusion front. To palliate this problem, the pour-out method was used. A mechanical probe senses the location of the melting front and rapidly drains the melt fraction at various moments of the melting process [14]. In addition, 17 thermocouples were used to measure the temperature distribution through the enclosure. Overall, three aspect ratios were studied ($A = 0.714,\ A = 0.5,\ A = 0.286$). Until recently, this experiment was the best available to test numerical models. Later, Wolff and Viskanta [26] carried a similar experiment with tin. However, for tin, the pour-out method was abandoned and only the mechanical probing and thermocouples were used. Two aspect ratios were studied ($A = 0.75,\ A = 1.0$). Later Beckermann and Viskanta [27] explored the impact of subcooling on the dynamics of the fusion process. A total of five experiments were carried out to cover a large range of temperature gradients. Again, gallium was used as its thermodynamic properties were well known and since it undergoes subcooling easily. Position of the steady-state melting front interface was used to test the model.

In 1984, another classical experiment was carried out by Bareiss and Beer [28]. They tracked the melting front in n-octadecane using photography and for three geometries: vertical wall, vertical cylinder, and horizontal cylinders. They presented results for two aspect ratios for $A = 1$ and $A = 0.5$ (40 mm and 20 mm in height). For a height of

71 mm ($A = 1.78$), they presented the evolution of the dimensionless molten mass and the Nusselt number for two values of ΔT (30.1 K and 11.1 K). A similar experiment was carried by Okada [29]. Again, n-octadecane was used in an enclosure 15 mm wide and 30 mm high. The position of the melt front was obtained by photography and the temperature distribution was measured along the centerline. Sourour et al. [30] studied the formation and the melting of a vertical ice slab subjected to a uniform heat flux boundary condition. The temperature distribution within the enclosure was measured with thermocouples.

Zhang and Bejan [31,32] carried a two-part study on the melting of n-octadecane in a rectangular enclosure. The first part was to study the melting without subcooling, and subcooling was the object of the second study. The enclosure was 74 cm high and 14.6 cm thick ($A = 5.07$). The width of the enclosure was set at 56 cm to minimize any three-dimensional effect. The temperature distribution in the liquid was measured with 55 thermocouples distributed at four levels. The shape of the melting front was also photographed.

Choi and Hong [33] studied the melting of n-octadecane in a rectangular enclosure of 16.5 cm high, 24.8 cm long, and 15.2 cm wide ($A = 0.67$). A wall of the enclosure was subjected to three different heat fluxes ($5.1 \times 10^3\,\text{W}\cdot\text{m}^{-2}$, $8.21 \times 10^3\,\text{W}\cdot\text{m}^{-2}$, and $10.92 \times 10^3\,\text{W}\cdot\text{m}^{-2}$). A total of 29 k-type thermocouples were installed at preselected locations in both the heating plate and the PCM. Nine different locations on the horizontal plane and at three heights were selected for the temperature measurements.

Campbell and Koster [13] designed an experiment on the melting and solidification of gallium. This experiment shares a lot of similarities with the classic acknowledged experiments [14,15]. However, they used a new technique based on radioscopy. This method makes use of gallium's increase (+3 %) in density in its liquid phase compared to its solid phase. This approach presents the major advantage of minimizing perturbations to the melting process caused by the pour-out method. The enclosure used was $1.25 \times 4.7 \times H\ \text{cm}^3$, where H was 1.4 cm and 3.3 cm to achieve aspect ratios of $A = 0.3$ and $A = 0.7$. In addition to X-ray measurements, five equally spaced k-type stainless steel sheathed thermocouples were used to measure the temperature inside the enclosure. As much as possible, the authors tried to reproduce the experimental parameters of [14,15]. They observed an intriguing interface shape when melting began, which they associated to some anomalous density properties of the gallium. In the freezing experiment, they observed that faster melting fronts were more rugged because of stronger convection and the dynamic of crystal formation.

Wang et al. [34] constructed an experimental setup for the melting of Polyethylene glycol 900 within a rectangular enclosure ($153 \times 103 \times 103\ \text{mm}^3$, $A = 0.67$). The two vertical side walls served as the heat source and sink, while the lateral walls were transparent to follow the melting front. The temperature distributions along the midplane, and top and bottom walls were measured using ten thermocouples which were unevenly distributed: that is closer near the heating plate and more distant near the heat sink. Experiments were carried out for five heat fluxes. This experiment suggested that there are three different regimes during the melting process. The conduction regime plays a dominant role during the initial stages of melting, and then a second regime appears in which convection dominates the heat transfer process. Between these two regimes lies the transition regime where both conduction and convection are prime factors in the melting process.

Silva et al. [35] used a rectangular enclosure for which the overall dimensions are 813 mm and 623 mm for total vertical and horizontal lengths. The two exchange plates were made of aluminum separated by a gap of 3 cm, while the two side walls were made of Plexiglas. One of the heat exchange plates was heated by an electrical element consisting of NiCr wires, while on the cold side, a forced air flow was used to keep the temperature constant. Temperature measurements were taken at three levels using four thermocouples placed through the thickness of the enclosure. The experiment was conducted at a constant heat flux of 480 $\mathrm{W{\cdot}m^{-2}}$.

The mass flow rate and the temperature of the cooling air were kept constant with values of 5.5 10^3 $\mathrm{kg{\cdot}s^{-1}}$ and 19.3 °C, respectively.

Reminiscent of the experiment of [13], Yin and Koster [36] used X-rays to study the melting and solidification of pure Al and Al-Cu alloy. Due to the high temperatures involved, the enclosures were made of boron nitride. Two specimen sizes were studied: $32 \times 32 \times 8\ \mathrm{mm^3}$ and $42 \times 32 \times 4\ \mathrm{mm^3}$. The broad sides of the sample faced the X-ray generator and the CCD camera used for X-ray detection, respectively. Molybdenum blocs were used to conduct heat flux generated by two boron nitride heaters, which produced a more uniform heat distribution. Thermocouples were placed in both molybdenum blocks (2) and in the melt phase (2 or 3).

Younsi et al. [37] studied the dynamics of the thermal behavior of a hydrated salt-based PCM. This material presents significant hysteresis, the melting point of which is 26.9 °C, while the crystallization temperature is 23.5 °C. This type of material is very challenging to characterize, since it is prone to subcooling and it is not a pure substance. In consequence, the properties change with the thermal cycles. This phase change material was enclosed in a $210 \times 140 \times 25\ \mathrm{mm^3}$ shell placed between two aluminum plates. Thermoregulated baths were used to control the temperature and fluxes. The plates were equipped with heat flux sensors and thermocouples. Unlike previous experiments, internal temperature distribution was not studied, since the objective of the experiment was to measure the thermal behavior through melting and freezing for a heat storage application.

Kumar et al. [38] pioneered the utilization of neutron radiography in the analysis of a melting block of lead. The melting front in a cuboid of $50 \times 50 \times 60\ \mathrm{mm^3}$ was tracked using a neutron source and a CCD camera equipped with a LiFeZnS converter.

Shokouhmand and Kamkari [39] studied the fusion of lauric acid, which belongs to the class of fatty acids, in a rectangular cavity measuring $50 \times 120 \times 50\ \mathrm{mm^3}$ and heated on only one side. Photographs of the front face of the tank and recorded temperatures along the low melting process were used to calculate the melt fraction, including the average Nusselt number on the hot wall. Results indicate that, in the initial stage of melting, heat conduction is the dominant mode of heat transfer, followed by the transition from conduction to convection regime. At the end of the melting process, the natural convection vanished.

Kamkari et al. [40] continued the previous experience and studied the dynamic behavior of the fusion of lauric acid in a rectangular tank at different angles. They show that as the inclination angle decreased from 90° to 0°, the convection currents in the enclosure increased and a chaotic flow structure appeared.

When melting starts in the horizontally inclined enclosure, the solid–liquid interface line becomes wavy, which induces the formation of Bénard convection cells in the liquid PCM and they found that the heat transfer enhancement ratio for the horizontal enclosure is more than two times higher than that of the vertical enclosure.

1.3 Need for More Experiments

Overall, even after more than 40 years, a surprisingly small number of experiments (27) have been carried out on the rectangular geometry. In addition, only a handful of materials have been studied, the most common being the n-octadecane (9 independent studies). It is worth noting that 45 % of the citations generated by the experiment on this peculiar geometry refer to the work of one research group (Viskanta et al.) and that this work was carried out in the 1980s. For this reason, the proposed work is part of a detailed experimental study of the behavior of paraffin during the melting process and the identification of the solid–liquid interface.

2 PCM Dynamic Behavior Introduction

For the experiment described here, paraffin is used. The material used belongs to the family of saturated alkane hydrocarbons (C_nH_{2n+2}) and is obtained from oil distillation. Such materials are environmentally safe, non-toxic, and relatively inexpensive. The thermophysical properties of the PCM for the solid and liquid phases are summarized in Table 1.

These thermophysical properties were experimentally determined: Measurements of specific heat, latent heat, and melting temperature were carried out using a calorimeter μDSC3. This technique uses a very small sample of material (<100 mg) to measure the differential heat flow in a reference material. The resulting thermogram obtained at a rate of $5\,^\circ\mathrm{C}\cdot\mathrm{min}^{-1}$ between 10 °C and 80 °C in both directions, heating and cooling, is presented in Fig. 1. Using this technique, the melting temperature of the PCM obtained was the intersection point between the tangent line of the largest peak of the DSC diagram.

The latent heats for phase transition are derived from the thermogram by numerical integration of the area under the peak of the DSC curve. The thermogram also allowed us to determine the variation of the liquid and solid heat capacity reported in Fig. 2.

Table 1 Paraffin global thermophysical properties

Parameters	Solid phase	Liquid phase	Uncertainty (%)
Melting point (°C)	52.1		0.4
Density $\rho(\mathrm{kg}\cdot\mathrm{m}^{-3})$	823	778	6.2
Latent heat $(\mathrm{kJ}\cdot\mathrm{kg}^{-1})$	153.27		3.0
Specific heat $(\mathrm{J}\cdot\mathrm{kg}^{-1}\cdot\mathrm{K}^{-1})$	2190 (at 20 °C)	2320 (at 70 °C)	4.8
Thermal conductivity $(\mathrm{W}\cdot\mathrm{m}^{-1}\cdot\mathrm{K}^{-1})$	0.27 (at 25 °C)	_	3.2

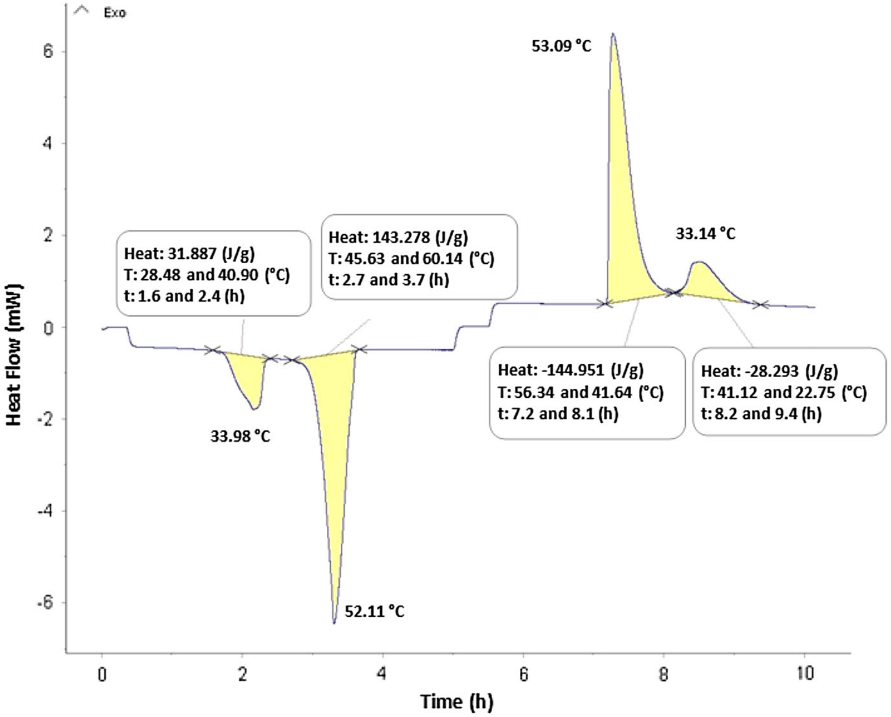

Fig. 1 Thermogram resulting of paraffin thermal heating program from 10 °C to 80 °C and cooling from 80 °C to 10 °C at a rate of 5 °C·min^{-1}

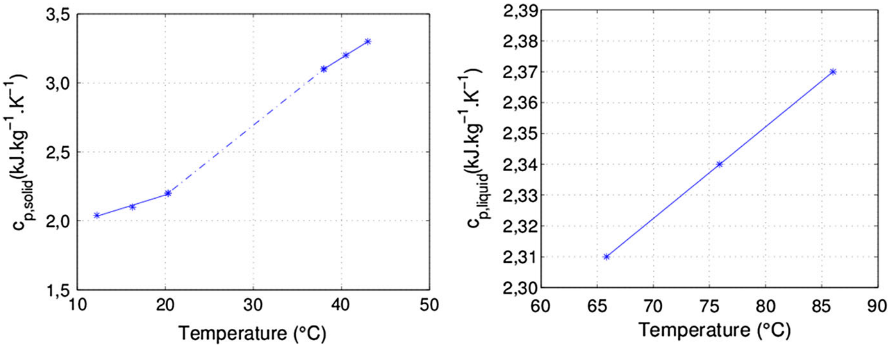

Fig. 2 Specific heat variation with temperature of: (*left*) the solid phase paraffin; and (*right*) the liquid phase paraffin

To measure the thermal conductivity of solid wax, an experimental device having a thin electrical resistance to provide a heat flow q'' was used. To measure the temperature T_c, a K-type thermocouple was installed between the polystyrene insulation of thickness e_i and a sample of MCP of thickness e.

All these components were sandwiched between two 4 cm thick aluminum blocks to ensure that the temperature remains uniform (Fig. 3).

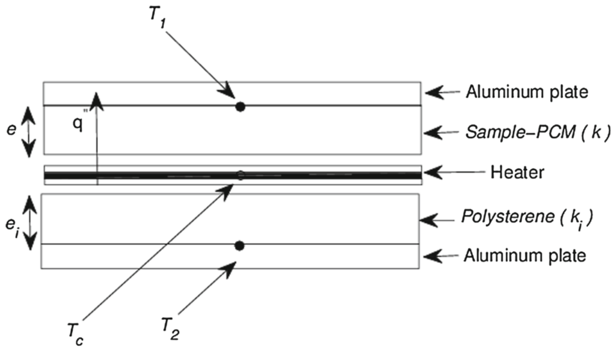

Fig. 3 Schematic diagram of the experimental setup

Two other similar thermocouples were located on the surface of the upper, T_1, and lower, T_2, aluminum block, which are in direct contact with the sample and the insulating material, respectively.

Heat flux q'' is divided into two flows q_1'' sample side and q_2'' from the insulating side:

$$q'' = q_1'' + q_2'' \tag{1}$$

The expression of each stream is given by Fourier's law:

$$q_1'' = k\ (T_c - T_1)/e \tag{2}$$

$$q_2'' = k_i\ (T_c - T_2)/e_i \tag{3}$$

and

$$k = e\left(\frac{q''}{T_c - T_1} - \frac{k_i}{e_i}\,\frac{T_c - T_2}{T_c - T_1}\right) \tag{4}$$

The thermal conductivity variation of the solid phase is shown in the graph of Fig. 4.

The density was measured using a glass tubular heat exchanger. The internal tube (15.94 mm of diameter) was filled with 20 g of paraffin. The external tube is connected to a thermostatic bath fixed at different temperature. For each change in temperature of the thermostat, the level of liquid paraffin was measured, and the volume density according to each temperature was determined. The density variation of PCM by temperature is shown in Fig. 5.

The measurement uncertainties were calculated using the method described by Barford [41].

2.1 Experimental Setup

The experimental setup intended for the measurement of the thermal response of PCMs was designed to impose uniform temperatures on both sides of a rectangular plane-

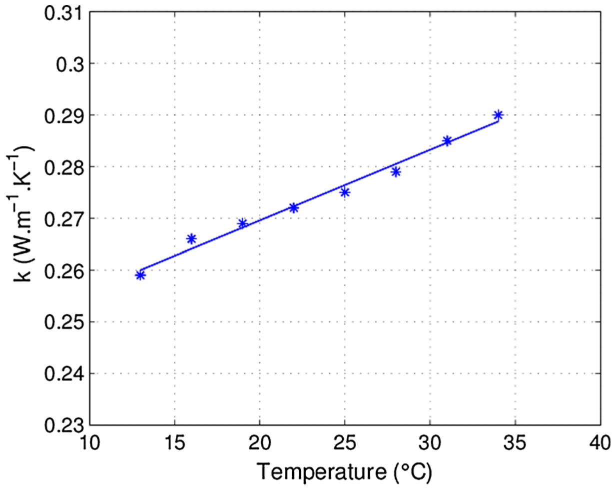

Fig. 4 Variation of the thermal conductivity with temperature of the sample

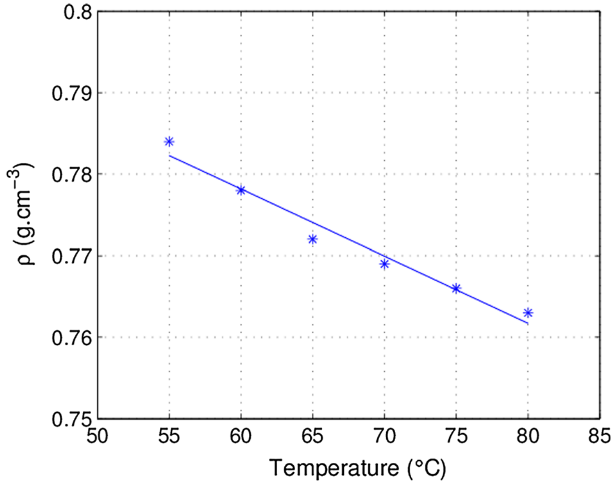

Fig. 5 Variation of the material density with temperature of the sample

parallel cavity filled with a phase change material. Here, a macroscopic approach to the measurements of the properties has been selected to obtain the real behavior of the material at the scale for which it should be used. The relatively large size of the sample provided an "effective" thermal response of the material, one that can determine the feasibility of the solutions. This section first describes the layout of the experimental bench and then discusses related issues in detail.

Figure 6 shows the details of the experimental bench. Twenty- five thermocouples are positioned within the PCM to examine its behavior and follow the melting/freezing front. In Fig. 6a, a close-up on the exchanger plates was presented.

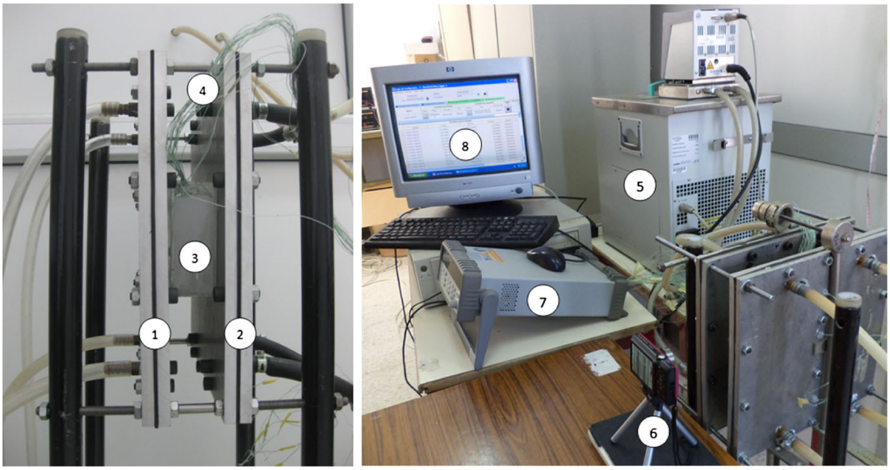

Fig. 6 Close-up and complete perspective of the experimental setup: (1) cold exchanger plate; (2) hot exchanger plate; (3) enclosure containing PCM; (4) wiring bundle of thermocouples; (5) thermostatic baths; (6) camera; (7) acquisition system; (8) computer

2.2 Heat Exchange Plates

There are several ways to impose the temperature conditions on a flat plate. The most common one involves bonding a coil on the external face of the plate and circulating fluid through this coil. However, the thermal contact between the coil and plate is often insufficient, which leads to a high thermal resistance between them. This makes it difficult to obtain a uniform temperature over the entire plate. However, it is critical to avoid any non-uniformity in temperature, because this can significantly affect the global heat flow [42].

To avoid this problem, the coolant was put in direct contact through a channel embedded into the plate. The channel was machined in a square ($300 \times 300\ \text{mm}^2$) 10 mm thick aluminum plate. A second 10 mm thick aluminum plate and a rubber seal were used to close the channel. Mechanical details are presented in Fig. 7. This liquid circulates in a closed circuit formed by the plate and a thermostat.

The thermostat is a thermo-regulated bath that is used to allow regulation of water injected into the exchanger plate with an accuracy of ±0.01 °C. This bath has a volume of 10 L and a heating power equal to 2000 W. The working temperature range is between 0 °C and 100 °C.

2.3 PCM Enclosure

The phase change material used was prepared in a tank of rectangular geometry ($200 \times 100 \times 50\ \text{mm}^3$). The front, back, top, and bottom plates are of Plexiglas (4 mm thick) to enable viewing of the phase change process. The plates are not in contact with the exchange plates to make them adiabatic. They have also been wrapped in insulation material. The two lateral plates are closed by the exchange walls and the PCM. An

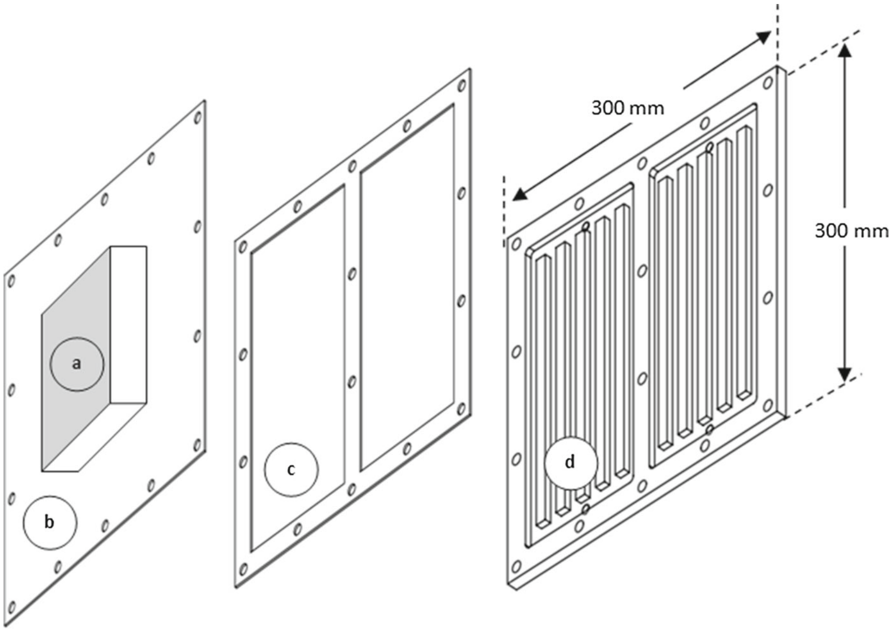

Fig. 7 Schematic of the heat exchange plates: (a) PCM enclosure; (b) aluminum plate used as cover; (c) rubber seal; (d) machined aluminum plate

area of air 5 mm thick is left between the PCM and the upper side of the tank to accommodate the density change during melting.

2.4 Automated Data Acquisition System

To measure the temperature profile of the sample as well as the exchange plates, 25 K-type thermocouples (sensitivity 4.0 µV for 0.1 °C) were used. They are positioned to measure the temperature distribution along the vertical middle plane. Figure 8 and Table 2 show respectively the positions and coordinates of the thermocouples in the sample. One should note that the position with respect to x is measured from the cold, that is the cold plate is at $x = 0$ and the hot plate is located at $x = 50$. These sensors are connected to a central multiplexer (Agilent 34970A) suited to measure the low voltage signals from the thermocouples. The multiplexer is connected to a computer via an RS-232 link. A program developed with the interface DATA-LOGGER 3 manages the acquisition and allows the transfer of data. For all of the tests, this acquisition software is used to track in real time the evolution of different measurements at 1 min intervals.

3 Operating Modes

3.1 Temporal Evolution of the Temperature of the PCM

The PCM is placed between the two exchange plates: tap water at T_c circulates in the cold plate and hot water at T_h in the hot plate. To measure the temperatures of the

Fig. 8 The actual thermocouples positions and coordinates

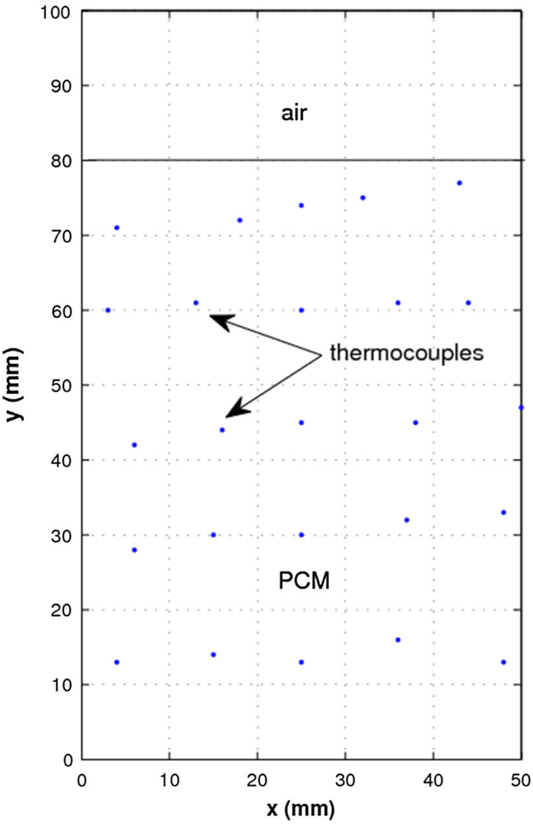

Table 2 Coordinates of thermocouples in the sample (x;y)

	(x;y) (mm)				
Level 5	(4;71)	(18;72)	(25;74)	(32;75)	(43;77)
Level 4	(3;60)	(13;61)	(25;60)	(36;61)	(44;61)
Level 3	(6;42)	(16;44)	(25;45)	(38;45)	(50;47)
Level 2	(6;28)	(15;30)	(25;30)	(37;32)	(48;33)
Level 1	(4;13)	(15;14)	(25;13)	(36;16)	(48;13)

plates and check their uniformity, thermocouples were installed in each of them. The evolution of the temperature of the PCM in the melting process is presented in Figs. 9 and 10.

Figure 9 shows the evolution of temperature with time for thermocouples located near mid-height in the cavity, that is for points located between $y = 42$ mm and $y = 47$ mm. Aside from the curve corresponding to the thermocouple coordinate (6;42), that is on the side of the cooled wall, the other curves reach the melting temperature of about 60 °C where the temperature stabilizes indicating the presence of the melting front. This temperature remains constant as there is still solid to melt in the cavity. The closer a point to the heated wall, the faster fusion will occur. For the

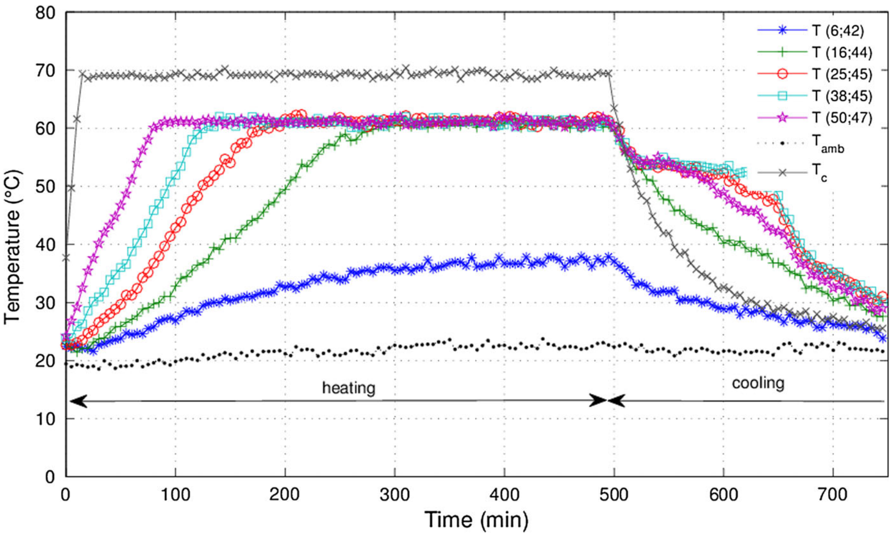

Fig. 9 Evolution of the temperature with time in the center of the PCM enclosure along the *horizontal axis*

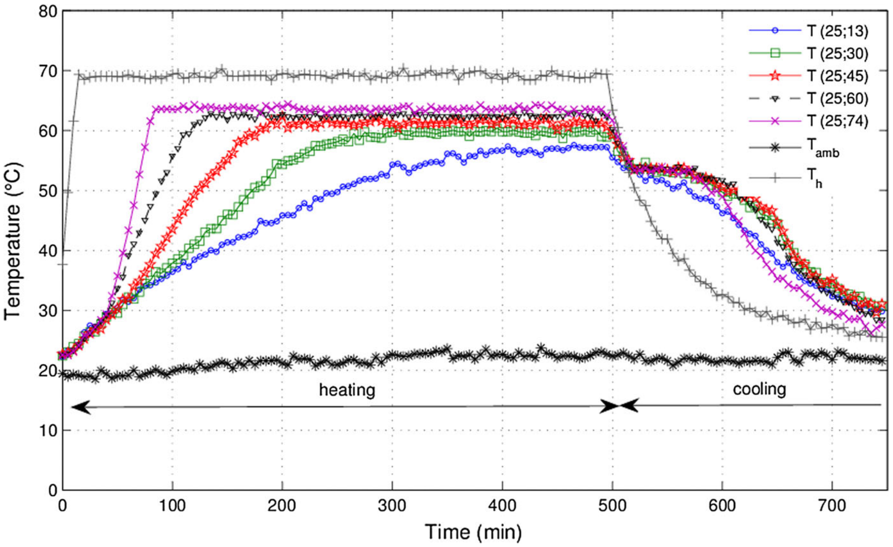

Fig. 10 Evolution of the temperature with time in the center of the PCM enclosure along the *vertical axis*

(50;47) point, fusion is detected after 85 min, while for the (16;44) location, fusion occurs only after close to 300 min. This provides a clear image for the melting front propagation along a horizontal axis.

Figure 10 shows the evolution of temperature with time for points located on the vertical line at the center of the cavity, $x = 25$. Figure 10 clearly indicates that the paraffin first melts near the top of the cavity. For instance, the first curve indicates that at location (25;74) near the top frontier, the PCM is melted at about $t = 85$ min, while

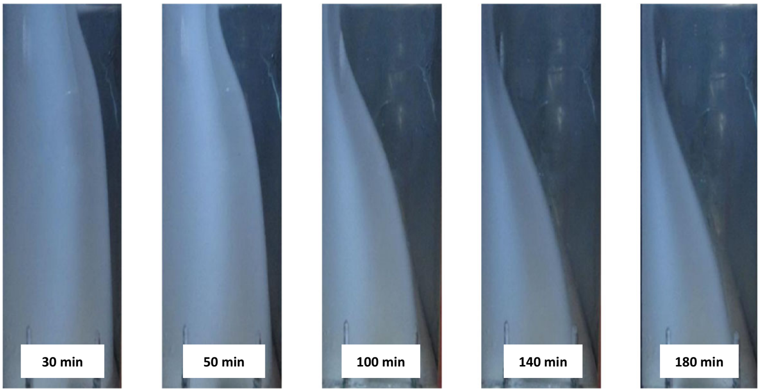

Fig. 11 Evolution with time of melting the front (from *right* hot plate to *left* cold plate) for $T_h = 70\,°\mathrm{C}$: Melting front visualization

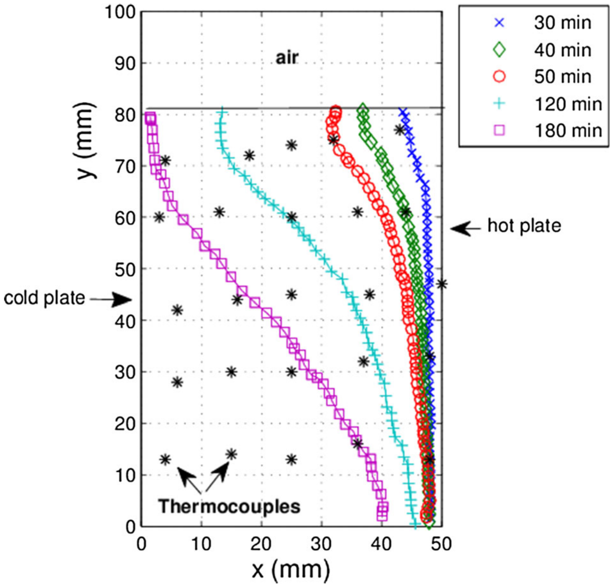

Fig. 12 Evolution with time of melting the front (from *right* hot plate to *left* cold plate) for $T_h = 70\,°\mathrm{C}$: Image processing

it is melted at about $t = 300$ min for location (25;30). This proves that the shape of the melting front is not parallel to the heated plate. Once heat supply is turned off, after 500 min, one can clearly see that supercooling occurs at about 53 °C, the recorded phase change temperature with the DSC (Fig. 1). For about 70 min to 80 min after the cutoff, the temperature remains constant at this temperature because solidification starts at constant temperature. Then, as the solid phase becomes preponderant, the temperature starts to decay to eventually reach the hot plate temperature. One could note that the upper point (25;74) shows a fast crystallization after $t = 500$ min as there is an important heat transfer with the air layer at the top of the cavity.

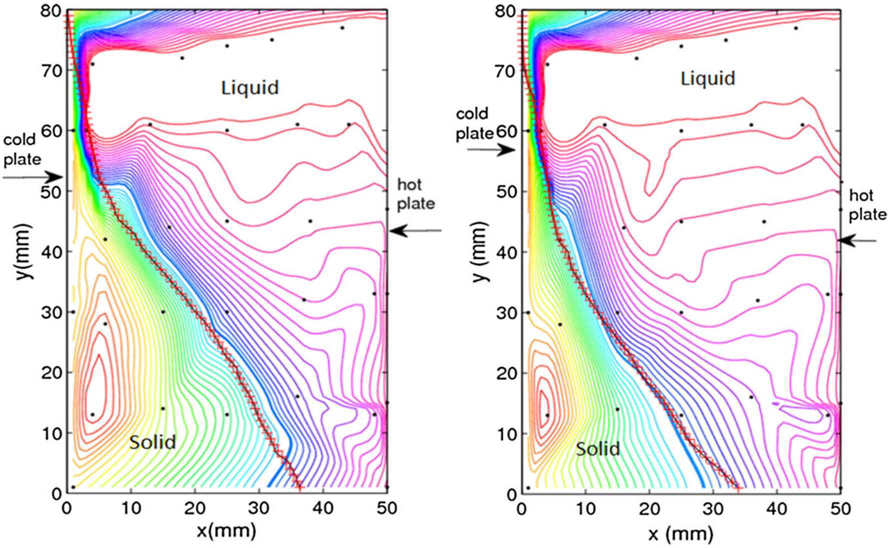

Fig. 13 Isotherms at two different instants in time for $T_h = 80\,^\circ\mathrm{C}$: (*left*) $t = 110$ min; (*right*) $t = 150$ min

3.2 Experimental Determination of the Melting Front by Image Processing

To confirm visually the above-mentioned results, Fig. 11 shows images of the cavity at different instants of time of the fusion process. These images are taken by a camera located perpendicularly in front of the cavity and they show the shape of the melting front during this process. The dark area is liquid paraffin, moving from the right to left with time in Fig. 11, and the light area is solid paraffin.

Image processing was performed on these pictures to obtain the melting front for different times between 30 min and 180 min of heating and the results are presented in Fig. 12. At the beginning of heating, a rectangular melt layer is formed between the PCM and the exchanger plate. Heat transfers are mostly due to conduction and the isotherms are vertical and parallel. Soon, convection begins in the upper right corner and melting is thus increased in the upper part of the enclosure. After 30 min, the melting front is no longer vertical, while after 180 min, the whole upper part is completely melted while the material at the bottom is only about 20 % melted close to the hot plate.

Figure 13 shows a complete representation of isotherms in the enclosure for $T_h = 80\,^\circ\mathrm{C}$ after (left) 110 min and (right) 150 min, respectively. These contours were produced using a cubic interpolation function in Matlab. Interpolations were obtained for a regular 50 mm × 80 mm Cartesian grid to produce the numerical values at every millimeter in the domain. In Fig. 13, the thermocouples (actual measurements) are shown, and the melting front itself is depicted by a continuous line (involving “x” symbols). Figure 13 shows the liquid bubble at the top ($y = 80$ mm) of the enclosure in both cases but also that air cools the liquid, therefore indicating thermal losses to the top of the apparatus.

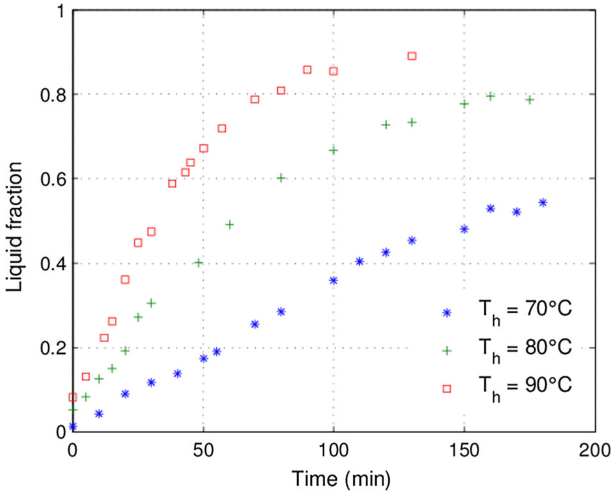

Fig. 14 Evolution with time of the liquid volume fraction of PCM for $T_h = 70\,^\circ\mathrm{C}$, 80 °C and 90 °C

Results presented in Fig. 13 will be quite useful in the upcoming research as numerical analysis will be carried out for the conditions and material investigated in the current work.

3.3 The Liquid Volume Fraction of PCM

Figure 14 shows the evolution of the liquid volume fraction in time for three different experiments: in the first one, the hot plate temperature is set to 70 °C while for the other two it is respectively 80 °C and 90 °C. The higher the hot plate temperature, the faster melting takes place. For $T_h = 70\,^\circ\mathrm{C}$, the heat propagates slower and the melted fraction increases more or less linearly with time (*). In the other two cases, the melt fraction increases more abruptly at the beginning and then the melting rate decreases. In these cases, rapidly, important convective flow occurs and the melting front area is important leading to important melting rates. But after a 50 % to 60 % melting, the remaining solid phase is harder to melt as the melting front surfaces decreases.

Wang et al. [34] proposed the following correlation for the liquid fraction, V/V_0, with respect to Fourier, Stefan, and Rayleigh dimensionless numbers. The correlation is also reported in Fig. 15 where $V/V_0/(\mathrm{Ste}^{1.538}\ \mathrm{Ra}^{0.002})$ is plotted against $\mathrm{Fo}^{0.906}$.

$$V/V_0 = 4.73\ \mathrm{Fo}^{0.906}\ \mathrm{Ste}^{1.538}\mathrm{Ra}^{0.002} \tag{5}$$

The experimental results of the present study have been represented in the same figure.

Figure 15 indicates that the trend is close with a vertical deviation. The present experimental results can be fitted with the following correlation. As the discrepancy between our experimental results and the correlation of Wang et al. does not exceed 9 %, it can be said that the proposed results confirm this correlation [34].

Fig. 15 Evolution with Fourier number of the melt fraction

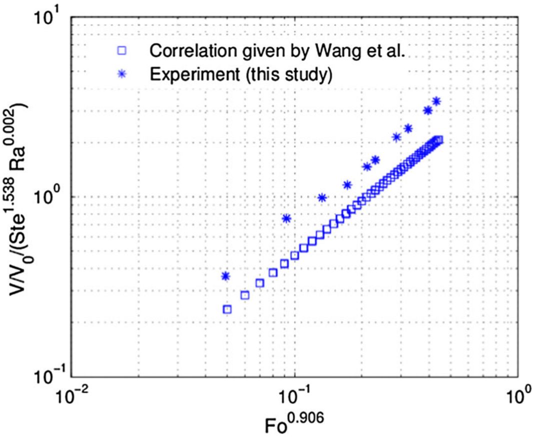

4 Conclusion

In this article, an experimental setup is used to study the dynamics of the melting process of a PCM in a rectangular enclosure. This paper's aim was to bridge the gap between the numerous numerical models available for the predictions of the PCM properties and this need for a comparison with experimental data. The objective was to carry out a high-quality experimental study to be used as a validation data source or as a standard reference to validate models.

The thermal behavior and geometric evolution in time of the melting front of paraffin have been determined experimentally for various temperatures on the hot boundary and several Fourier numbers. The superposition of the melting front determined by thermocouples placed in the center of the tank with that determined by pictures taken by a camera shows a small deviation due to the uncertainty on the exact position of thermocouples and camera. Nevertheless, excellent agreement was obtained.

The study of the liquid fraction variation in time allows inferring that the reported melt and solid volumes depend on the difference between the imposed boundary temperatures and the fusion temperature of the material.

In a following work, the data obtained from this experiment will be used to assess the validation of the formulation a numerical method.

Acknowledgments The authors gratefully acknowledge the Natural Sciences and Engineering Research Council of Canada (NSERC) for financial support. The authors also thank the partners of the t3e research group, who support the project.

References

1. A. Sharma, V.V. Tyagi, C.R. Chen, D. Buddhi, Renew. Sustain. Energy Rev. **13**, 318 (2009)
2. F. Agyenim, N. Hewitt, P. Eames, M. Smyth, Renew. Sustain. Energy Rev. **14**, 615 (2010)
3. R. Baetens, B.P. Jelle, A. Gustavsen, Energy Build. **42**, 1361 (2010)
4. M.M. Kenisarin, Renew. Sustain. Energy Rev. **14**, 955 (2010)
5. L.F. Cabeza, A. Castell, C. Barreneche, A. De Gracia, A.I. Fernández, Renew. Sustain. Energy Rev. **15**, 1675 (2011)
6. F. Kuznik, D. David, K. Johannes, J.J. Roux, Renew. Sustain. Energy Rev. **15**, 379 (2011)

7. E. Oró, A. De Gracia, A. Castell, M.M. Farid, L.F. Cabeza, Appl. Energy **99**, 513 (2012)
8. D. Zhou, C.Y. Zhao, Y. Tian, Appl. Energy **92**, 593 (2012)
9. A. Waqas, Z. Ud Din, Renew. Sustain. Energy Rev **18**, 607 (2013)
10. Y. Dutil, D. Rousse, N.B. Salah, S. Lassue, L. Zalewski, Renew. Sustain. Energy Rev. **15**, 112–130 (2011)
11. Y. Dutil, D. Rousse, S. Lassue, L. Zalewski, A. Joulin, J. Virgone, F. Kuznik, K. Johannes, J.-P. Dumas, J.-P. Bédécarrats, A. Castell, L.F. Cabeza, Renew. Energy **61**, 132 (2014)
12. N. Hannoun, V. Alexiades, T.Z. Mai, Num. Heat Transf, Part B: Fundam **44**, 253 (2003)
13. T.A. Campbell, J.N. Koster, J. Cryst. Growth. **140**, 414 (1994)
14. C. Gau, R. Viskanta, Int. J. Heat Mass Transf. **27**, 113 (1984)
15. C. Gau, R. Viskanta, J. Heat Transf. **108**, 174 (1986)
16. I. Wintruff, C. Günther, A.G. Class, Numerical Heat Transfer, Part B: Fundam. **39**, 127 (2001)
17. O. Bertrand, B. Binet, H. Combeau, S. Couturier, Y. Delannoy, D. Gobin, M. Lacroix, P. Le Quéré, M. Médale, J. Mencinger, H. Sadat, G. Vieira, Int. J. Therm. Sci. **38**, 5 (1999)
18. D. Gobin, P. Le Quéré, Comp. Ass. Mech. Eng. Sci. **7**, 289 (2000)
19. J. Szekely, P.S. Chabra, Metall. Mater. Trans. B. **1**, 1195 (1970)
20. F.M. Chiesa, R.I.L. Guthrie, J. Heat Transf. **96**, 377 (1974)
21. R.H. Marshall, Therm. Storage. Heat Transf. Solar Energy Syst. 61 (1978)
22. N.W. Hale, R. Viskanta Jr, Lett. Heat Mass Transf. **5**, 329 (1978)
23. V.P. Carey, B. Gebhart, J. Fluid Mech. **107**, 37 (1981)
24. P.D. Van Buren, R. Viskanta, Int. J. Heat Mass Transf. **23**, 568 (1980)
25. C.-J. Ho, R. Viskanta, J. Heat Transf. **106**, 12 (1984)
26. F. Wolff, R. Viskanta, Int. J. Exp. Heat Transf. **1**, 17 (1987)
27. C. Beckermann, R. Viskanta, J. Heat Transf. **111**, 416 (1989)
28. M. Bareiss, H. Beer, Int. Commun. Heat Mass transfer. **11**, 323 (1984)
29. M. Okada, Proc. ASME/JSME Therm. Eng. Jt. Conf. **1**, 281 (1983)
30. M.M. Sorour, M.A. Hassab, M.B. Madi, F.T. Kandil, Int. Commun. Heat Mass Transf. **14**, 167 (1987)
31. Z. Zhang, A. Bejan, J. Heat Mass Transf. **32**, 1063 (1989)
32. Z. Zhang, A. Bejan, Int. J. Heat Mass Transf. **32**, 2447 (1989)
33. K.J. Choi, J.S. Hong, Int. J. Exp. Heat Transf. **3**, 49 (1990)
34. Y. Wang, A. Amiri, K. Vafai, Int. J. Heat Mass Transf. **42**, 3659 (1999)
35. P.D. Silva, L.C. Goncalves, L. Pires, Appl. Energy **73**, 83 (2002)
36. H. Yin, J.N. Koster, J. Alloy. Compd. **52**, 175 (2003)
37. Z. Younsi, L. Zalewski, S. Lassue, D. Rousse, A. Joulin, Int J. Thermophys. **32**, 674 (2011)
38. L. Kumar, B.S. Manjunath, R.J. Patel, S.G. Markandeya, R.G. Agrawal, A. Agrawal, Y. Kashyap, P.S. Sarkar, A. Sinha, K.N. Iyer, S.V. Prabhu, Int. J. Therm. Sci. **61**, 15 (2012)
39. H. Shokouhmand, B. Kamkari, Exp. Therm. Fluid. Sci. **50**, 201 (2013)
40. B. Kamkari, H. Shokouhmand, F. Bruno, Int. J. Heat Mass Transf. **72**, 186 (2014)
41. N.C. Barford, in *Experimental Measurements: Precision, Error and Truth*, 2nd edn, Repr. (Wiley, Chichester, 1990)
42. B. Binet, M. Lacroix, Int. J. Numer. Method. Heat. Fluid Flow **10**, 286 (2000)